Monthly Notices
of the
ROYAL ASTRONOMICAL SOCIETY

MNRAS **436,** 2722–2733 (2013) doi:10.1093/mnras/stt1771
Advance Access publication 2013 October 15

Reducing Si population in the ISM by charge exchange collisions with He^+: a quantum modelling of the process

M. Satta,[1]⋆ T. Grassi,[2] F. A. Gianturco,[2]⋆ S. A. Yakovleva[3] and A. K. Belyaev[3]

[1]*CNR-ISMN and University of Rome 'Sapienza', P. le A. Moro 5, I-00183 Rome, Italy*
[2]*Department of Chemistry and CNISM, University of Rome 'Sapienza', P.le A. Moro 5, I-00161 Rome, Italy*
[3]*Department of Theoretical Physics and Center for Advanced Study, Herzen University, St. Petersburg 191186, Russia*

Accepted 2013 September 18. Received 2013 September 18; in original form 2013 July 1

ABSTRACT

The possible losses of silicon atom population during star-forming evolution and in the (photon-dominated region) PDR environments of the interstellar medium (ISM) can have different origins, one being the charge exchange (CE) encounter with the helium cations ($Si + He^+$) one of the most abundant species in those environments. This work investigates the different features of the likely interaction potentials leading to asymptotic partners like Si, Si^+, Si^{++} and He or He^+, in order to determine the influence of more accurate cross-sections on the chemical evolution of the ISM. We analyse the behaviour of interacting Si and He atoms by using ab initio quantum molecular methods. To obtain the corresponding transition probabilities, we employ a simple sequential grouping of single-crossing Landau–Zener events, and the time-dependent rate coefficients for the CE processes involved are obtained over a broad range of the gas temperatures. The results are seen to differ substantially from an earlier Langevin-type modelling of such process and further suggest a much more complex variety of possible molecular evolution mechanisms. We find, in fact, the unexpected presence of electron shake-off effects leading to Si^{++} generation yielding to emission of an electron, which has never been considered before and that, although with markedly smaller cross-sections, can indeed contribute to Si losses after the primary CE event. The consequences of these novel findings are tested on evolutionary model calculations and the results discussed in detail.

Key words: atomic processes – molecular processes – ISM: evolution.

1 INTRODUCTION

The chemical/molecular aspects of the changes occurring in the interstellar medium (ISM) and within the atmospheres of emerging planets are all critical elements for our understanding of the actual evolutionary paths which are being followed in order to generate the final abundances of such species. Their outcomes can in turn be compared with existing data obtained by observations (e.g. see Glover et al. 2010; Yamasawa et al. 2011) and therefore are clearly linked to the initial abundances of the chemical elements, to the various chemical transformations which are open to each of them under the macroscopic conditions of the environments (e.g. temperature, pressure, background radiation content, level of atomic ionization, etc.) to the relative probabilities of their physical evolutions and to the relative efficiencies of the formation/destruction paths present within the network in question (e.g. see Grassi et al. 2012).

⋆E-mail: mauro.satta@uniroma1.it (MS); francesco.gianturco@uniroma1.it (FAG)

More specifically, to be able to realistically determine the large data base of reaction rate coefficients which are associated with the formation or the destruction of each composing element, or composing molecular species, directly poses the question of being able to set up either an experimental machinery or a computational/theoretical simulation that could provide such information. This means that, at least at the computational level, one has to understand the elementary mechanism through which the specific molecular evolution occurs and further obtain the related nanoscopic quantities which play a role in determining that rate.

Once such a task is satisfactorily completed, however, one then needs to solve the large system of coupled first-order-differential equations (ODEs) that shall describe the network evolution, thereby having to face an often demanding computational task involving several thousands of linked chemical process (Grassi et al. 2012) that control the evolutionary history of that network.

In the present study, we shall address both aspects of the above problem by trying to provide a computational answer to the question of the disappearance of atomic silicon, a process which is expected to play an important role in the study of the ISM environments that

exhibit a locally small UV flux, i.e. which have become optically thick, so that the possible presence of metals like Si is not yet associated with a large number of photon-dominated region (PDR)-provided Si atomic ions, while also having a non-negligible ion density due to the presence of cosmic rays with the correct energy content.

The possibility of undergoing population losses via different dynamical paths for the present title metal is therefore linked, among other things, to its interaction with the most abundant atomic cation existing in the ISM, i.e. the $He^+(^2S)$ partner. In other words, we wish to examine the likely molecular steps for the mechanism of the charge exchange (CE) process given by

$$Si(^3P) + He^+(^2S) \rightleftharpoons Si^+(^2P) + He(^1S)\,, \qquad (1)$$

where the actual state of the final Si^+ product is considered to be its ground electronic state.

The above destruction process is very exothermic due to the large energy difference between the ionization potential of the He partner (24.5874 eV) and the same quantity for the Si atom (8.1517 eV), so that more than 16 eV (i.e. 16.43 eV) are available for redistribution after the CE process of equation (1). This extremely large difference means, at the molecular level, that there are several possible final channels which become energetically open and therefore different features of that process can play a significant role. The main ones are briefly listed below:

(i) the dynamics of the collisional CE event implies a sequence of non-adiabatic electronic effects, which act chiefly at the possible crossings in configurational space of the several diabatic, Born–Oppenheimer electronic potential energy curves (PECs) associated with the initial entrance channel and the electronically excited CE outgoing channels, which subsequently will decay into the much lower final exit channel of equation (1);

(ii) it is in fact clear that, because of the large energy gap existing between the above asymptotic partners, the only exit channels which could have non-adiabatic crossings with the initial PEC correspond to electronically excited Si^+ atoms: the excitation energy of He, in fact, is $\sim$19 eV, hence well above the crossing regions;

(iii) we therefore expect to see a large number of excited Rydberg-like states of $[Si^+]^*$ to be involved in the intermediate CE channels; they could then cross non-adiabatically the primary entrance channel of equation (1), thereby transferring excitation from the environmental He cations to the newly formed silicon cation that is also electronically excited; and

(iv) all the above states can therefore converge to another silicon configuration for which the adiabatic potential curves are located intermediately within the two channels of equation (1), causing an electron shake-off process whereby silicon double ionization occurs after the crossing

$$Si(^3P) + He^+(^2S) \rightarrow Si^{++}(^1S) + He(^1S) + e^-. \qquad (2)$$

Hence a doubly charged ion is produced *below* the PEC of the entrance channel. One should notice, in fact, that the second ionization potential of Si is 16.34 eV, thus placing the dication formation still well above the final channel of the ground states of Si cations and He atoms, as we shall discuss below. The latter non-adiabatic path, which produces one electron into the continuum while another electron has migrated on to the He cation, therefore needs to be taken into consideration.

From the above, sketchy analysis of the electronic states which are likely to be involved, it therefore follows that the destruction mechanism of Si atoms by collisional CE could evolve along a series of steps.

(i) Charge transfer with ion excitation: a non-adiabatic region with several Rydberg-like states of the $[[Si^+]^* + He(^1S)]$ system with final formation of excited ions of silicon. The latter species could then become stabilized by radiative emission into the final ground electronic states of the Si cation.

(ii) Charge transfer plus ionization: non-adiabatic transitions with the one electron shake-off channel when doubly charged silicon cation is produced and one electron is emitted into the continuum: such channel also contributes to the disappearance of Si atoms.

The above brief discussion clearly points at a greater variety of non-adiabatic crossings than previously envisaged from the simple occurrence of a possible crossing between the initial and final channels of equation (1). In the following sections, we will therefore describe the calculations of the necessary electronic PECs, the mechanism of collisional, non-adiabatic CE processes and the calculations of the corresponding transition probabilities from which we obtain the partial cross-sections. The latter will be in turn employed to generate the total reaction rate coefficients for production of both singly and doubly charged ions of silicon atoms. Our next step will further be to assess the effects of the Si destruction rates obtained by this work on the modelling of the evolutionary path where earlier data have been employed (Le Teuff, Millar & Markwick 2000) to study the same evolution. Our final conclusions will be presented in the last section.

2 THE MODELLING OF THE POTENTIAL CURVES

The level of calculation of the PECs has been chosen so as to realistically describe the high energy excited levels of the Si^+ which are present at the crossings. Current, high-correlated multireference methods are not as yet able to give reasonable results for highly excited Rydberg states as in the present process, hence we have adopted a more approximate, but still feasible, strategy to produce numerical estimates of the PECs involved in the various CE processes. The doublet and quartet ground states of the $Si(^3P)$+$He^+(^2S)$ have been calculated in the framework of the constrained density functional theory (DFT) formalism of Wu & Van Voorhis (2005), using the B3LYP density functional (Becke 1993) and building the initial wavefunction as having the positive charge confined to be on the helium atom. The aug-cc-pVTZ correlation consistent polarized basis set developed by Dunning (1989) was employed for all calculations. The Basis-set-superposition-error effects have been tested by employing the counterpoise procedure (Boys & Bernardi 1970), and negligible changes have been observed, as expected for the case of ionic partners. The scan of the relevant PEC was conducted with a step of 0.05 Å for the distances from Si to He below 3.0 Å and with steps of 0.2 Å for distances above 3.0 Å, the overall distance ranging from 1 to 12 Å. The PECs for the ground state $Si^+(^2P)$+$He(^1S)$ and the double charged state $Si^{++}(^1S)$+$He(^1S)$ were calculated at the same level of accuracy as above but without any charge localization constraint. The PECs for the Rydberg states $[Si^+]^*$+$He(^1S)$ were estimated by shifting the asymptotic values of the PEC of $Si^{++}(^1S)$+$He(^1S)$ using the atomic energy levels of Si^+ relative to the double charged state of Si [i.e. $Si^{++}(^1S)$], taking the relevant atomic energies from existing data base (Martin & Zalubas 1983; Kramida et al. 2013). This approximate scheme finally yields 27 PECs each of which crosses the initial curve of $Si(^3P)$+$He^+(^2S)$, as we shall further discuss below. The crossings at smaller distances

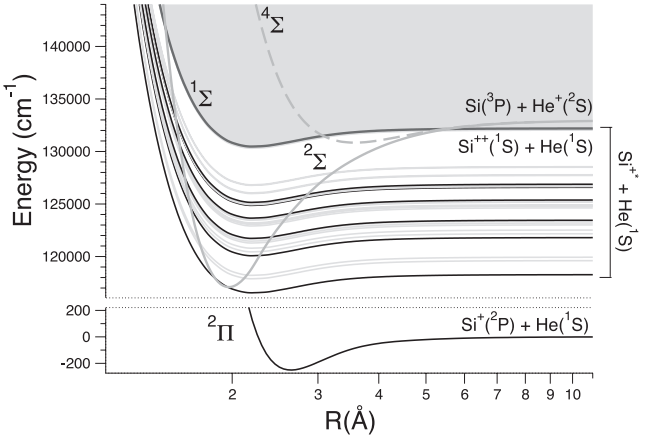

Figure 1. PECs for the (He-Si)$^+$ CE process discussed in this work. Selected crossings which are allowed by the symmetry of the overlap factor in equation (B16) are represented as thick lines reporting the surviving crossing.

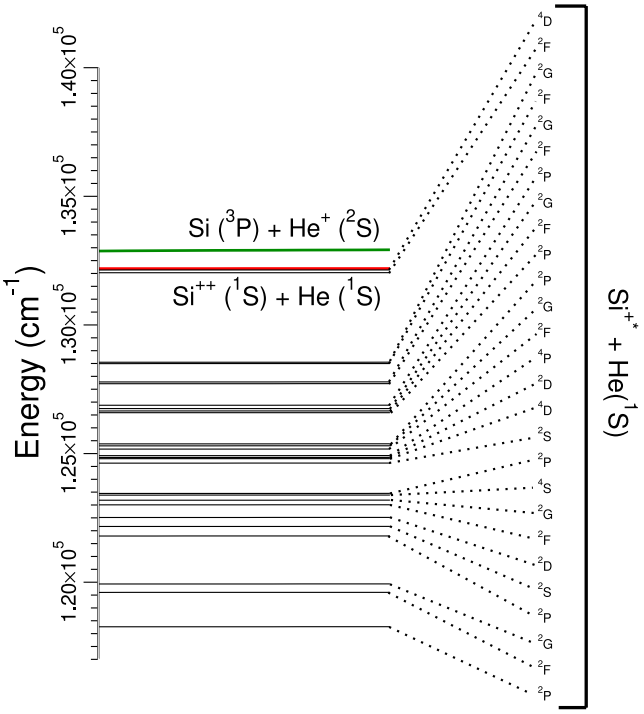

Figure 2. Atomic energy levels (Kramida et al. 2013) of Si^+ used in this work to shift the $^1\Sigma$ PEC of $SiHe^{++}$ in order to obtain the molecular Rydberg PEC of $(SiHe)^{+*}$.

than 2 Å have been defined as 'inner crossings', the others being the 'outer crossings'. The plots of Fig. 1 provide an overall view of the relevant processes involved in the present mechanism for CE between Si atoms and He^+ cations. The entrance partners in the interaction region form the $^2\Sigma$ and $^4\Sigma$ molecular curves of the $(SiHe)^+$ system, which are seen to be clearly located above the shake-off $^1\Sigma$ potential whereby the silicon dication is formed and one bound electron is ejected into the continuum. One should mention here that the spectroscopic notations we use involve the spin–orbit couplings between the bound electrons. If that coupling is further correctly extended to the continuum electron, then the outgoing curve becomes a $^2\Sigma$ for that exit channel. We shall further discuss this point below. Such states exist here embedded into the manifold of lower lying Rydberg states of the excited cation Si^+ interacting with the neutral He atom. Their spectroscopic labels and relative energy location are reported by the levels listed in Fig. 2. We clearly see there the presence of a closely packed multitude of levels converging above to an electron ejection process following the primary CE process. The entrance partners in the interaction region form also the $^2\Pi$ and $^4\Pi$ molecular curves of the $(SiHe)^+$ system: these are the first excited states of the relative Σ curves, and cannot be reliably calculated within the framework of the constrained DFT formalism employed in this work. One should note, however, that both the $^2\Pi$ and $^4\Pi$ interaction channels correspond to the formation of more weakly bound $(SiHe)^*$ states where the electronic excitation to the unoccupied molecular orbitals with π-character requires energy increases that we estimate, at the equilibrium, to be between 3 and 5 eV for the present cases. Hence, such channels are expected to generate PECs that are higher in energies with respect to the $^4\Sigma$ channel and will not cross the relevant CE states of Fig. 1. The details of the new physics which is now involved will be further discussed in the following sections.

3 THE CHARGE EXCHANGE MECHANISM: A MULTITUDE OF LANDAU–ZENER CROSSINGS

The previous discussion has already revealed that the diatomic molecular cation $SiHe^+$ is a very interesting species because the asymptotic energy of the partners for the case in which the ionic charge is kept on the He atom corresponds to having nearby highly excited electronic states of the silicon partner cation, while the cases where the charge is transferred on to the Si ground state ion, and therefore a large amount of energy (as discussed before, about 16.45 eV) is recovered, are located much lower in energy and well away from any possible crossing feature. In other words, and as already mentioned in Section 1, a multitude of intermediate cationic states exist below the primary entrance channel of the Si and He^+ and must correspond to singly ionized Si atoms in highly excited electronic states interacting with neutral He in its ground electronic state. Furthermore, given the fairly small second ionization potential of the Si, it follows that the doubly ionized states of $Si^{++}(^1S)$ interacting with $He(^1S)$ can form in the short range of relative distances and remain located below the primary asymptote of Si + He^+. The crossings between the above channels therefore produce an intermediate product whereby the neutral Si atoms are still destroyed at the expenses of the He cations but an additional electron is emitted, and the final systems will therefore decay through a variety of possible processes that we shall not specifically discuss in this study since they will always be those producing additional losses of neutral Si atoms, our primary interest here. The Si^{++}+He curve at distances $R < 5$ Å (see Fig. 1) crosses the $^2\Sigma$ entrance channel and does it again at around 1.5 Å thus forming a weakly bound $(SiHe)^{++}$ species, as illustrated by Fig. 1: it will play a role in our discussion below. One should further mention here that, as outlined before, the actual inclusion of the spin–orbit coupling with the continuum electron creates a different spectroscopic notation for the $(SiHe)^{++}$ curve: as it gives rise to a $^2\Sigma$ state. If there is no spin–orbit coupling included in our equations, then the $^4\Sigma$ will not cross the $^2\Sigma$ of the other channel. However, such cross-sections are expected to be very small within our simplified scheme, so the final result will be nearly the same as cancelling such contributions, a feature which shall also allow us to check the computational reliability of the dynamical model discussed in Appendix B. Thus, our present modelling of the non-adiabatic dynamics will treat the

$(SiHe)^{++}$ curve as being approximately $^1\Sigma$ with its correct coupling with the $^2\Sigma$ curve of the $(SiHe)^+$ entrance channel.

In summary, the mechanism for depleting the silicon atom populations by a CE with ionization process involving He^+ cations chiefly involve two different molecular paths, i.e. the excitation into the Rydberg-like Si cations:

$$Si + He^+ \rightarrow \left(Si^+\right)^* + He, \tag{3}$$

which can then radiatively decay into the stable ground state species:

$$\left(Si^+\right)^* \rightarrow Si^+\left(^2P\right) + h\nu, \tag{4}$$

or the direct CE + ionization process induced by the initial CE event, as described by equation (2),

$$Si + He^+ \rightarrow \left(Si^{++}\right) + He + e^-, \tag{5}$$

which we call here a shake-off process caused by the non-adiabatic crossing between the $^2\Sigma$ and $^4\Sigma$ states of $(SiHe)^+$, embedded now into the electronic continuum of one emitted electron of Si.

The quantum and semiclassical treatments involved in the dynamics of excitation transfer and CE plus ionization processes similar to those given by equations (3) and (5) have been clearly discussed long ago by Miller (1970) and Miller & Morgner (1977). They described these processes by a unified theoretical model which we have followed in our calculations, as discussed in greater detail in the present Appendix B.

One should further mention here that, in terms of multiplicity of states, the previous $^2\Pi$ and $^4\Pi$ channels excluded from contributing to the CE processes absorb about 6/9 of the total flux. However, the variety of multiple crossing indicated by Fig. 1 is referring to only one component of the interacting $Si(^3P)$ state, while the outgoing channels with the Rydberg ionic partner that are allowed by symmetry considerations (see discussion below) are all ^2P states which in the scheme of Fig. 2 have always two components ($J = 1/2$ and $3/2$). All the curves shown by Fig. 2 should therefore be split, each generating two close potential curves: they will increase the number of crossings occurring for the Rydberg states of Si^{+*}. We shall argue that it is more realistic to treat both flux variations (reduction because $^2\Pi$, $^4\Pi$ exclusion and increase because of ^2P multiplicity effects) within the present modelling of the CE processes.

We discuss in great detail in Appendix A the rather involved procedure followed in accounting for the physical presence of multiple crossings between the potential curves obtained above. We also employed a detailed quantum method to extract from such crossings the final CE cross-sections and we discuss in Appendix B of this paper the theoretical and numerical procedures we have selected to obtain our results. The next step is therefore that of defining our CE rates, as done below.

4 CROSS-SECTIONS AND RATE CONSTANTS

The probabilities for non-adiabatic crossings into the Rydberg states of the silicon single cation are given by the formulae of equations (A1)–(A12) discussed below in our Appendix A. Both the individual probabilities for the Penning-like shake-off process and those from the multiple crossing Landau–Zener (LZ) model need now to be integrated over the impact parameter b to yield partial cross-sections for the composite processes of Appendices A and B, equations (3 B) and (2 B)

$$\sigma_\ell(v) = 2\pi \int_0^\infty b\, \mathrm{d}b\, \hat{P}_\ell(b). \tag{6}$$

In conclusion, therefore, there will be two different sets of contributions to the final cross-sections for the depletion of Si atom populations via CE processes involving He^+: the shake-off cross-sections associated with reaction (2), the $\sigma_{\mathrm{shake-off}}(v)$ and the depletion cross-section linked to the LZ transition into cationic Rydberg states given by equation (3), the $\sigma_{\mathrm{Ryd}}(v)$. Note that, since each ^2P has two states ($J = 1/2$ and $3/2$), we must always perform a sum over the two components in the equation (7) reported below.

After integration over the range of b values, since the partial cross-sections are a function of the relative velocity v, the final cross-sections are obtained by sum over all the crossing processes and further integrated over their relative velocities to obtain the rate constants as a function of the ISM temperature T:

$$k_{\mathrm{CE}}(T) = 4\pi \left(\frac{\mu}{2\pi KT}\right)^{3/2} \int \sum_\ell g_\ell^i \sigma_\ell(v) v^3\, \mathrm{e}^{-\frac{\mu v^2}{2KT}}\, \mathrm{d}v, \tag{7}$$

where g_l^i is the statistical weight for the population of the entrance channel: which is 1/9 for the $^2\Sigma$ and 2/9 for the $^4\Sigma$ state, having neglected the 4/9 contribution of the $^4\Pi$ and 2/9 contribution of the $^2\Pi$ state, as specified in Section 2. The latter quantities will then be used within the evolutionary modelling described in Section 6.

One should note here that the above averaging over velocities also ensures that possible shifts on the crossing positions, caused by using different ab initio curves are spread over the relevant range of energies, thus making the final rates less sensitive to these corrections and thus more robust with the respect to the selected PECs.

5 PRESENT RESULTS

5.1 The CE partial cross-sections

The structural and energy parameters produced within the model of the previous section, and employing all the PECs discussed in Section 2, are used to generate the partial cross-sections for the processes of the present study. The energy dependence of the partial cross-sections pertaining to the shake-off process of equation (2), and involving the $^2\Sigma$ PEC in the entrance channel, is shown by the data in Fig. 3. Such data should be considered as upper limit estimates because of the present simplifications introduced in the

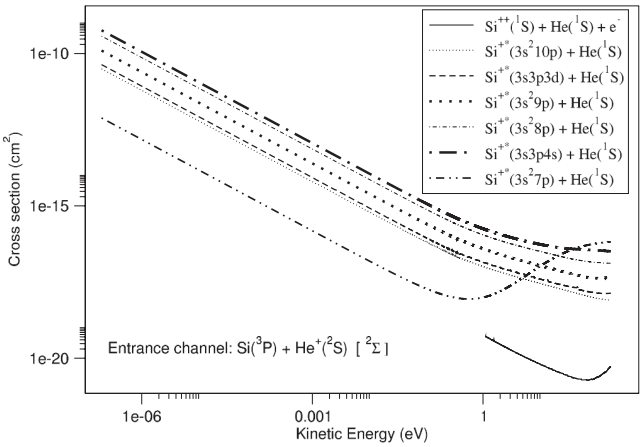

Figure 3. Computed CE cross-section for the doublet entrance channel (see Figs 1 and 2). The key reports the variety of exit channels due to the allowed crossings with the dication production (shake-off) and Rydberg states Si^+ manifold.

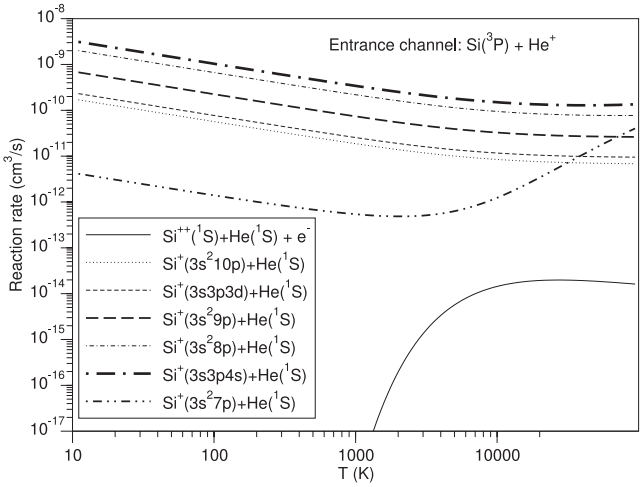

Figure 4. Computed doublet (CE+electron emission) non-adiabatic rates as a function of temperatures.

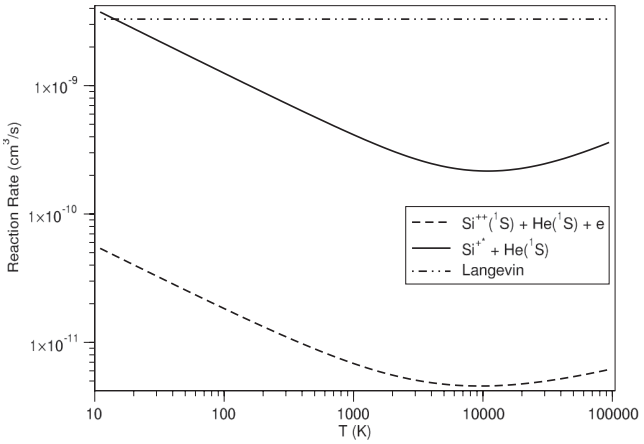

Figure 5. Computed rates for the total production of silicon cations by CE processes between Si atoms and He^+. The Langevin modelling is given by the top curve (Le Teuff et al. 2000). See the text for further details.

dynamical treatments, as discussed in detail in Appendix B given below.

One notices clearly the marked difference in size when the shake-off process is driven by the non-adiabatic CE outer crossing at the larger relative distances of about 5 Å: the overlap integral in equation (B16) is obviously much smaller at such large distances of interaction and therefore the corresponding width tends to zero, thereby efficiently recombining the active electron. One should be reminded here that, in the case of the $^4\Sigma$ entrance channel, these cross-sections are strictly zero when the spin–orbit coupling is not included: we have also calculated them using the same present model as done for the data in Fig. 3 to confirm, as we found indeed that they correctly came out numerically to be very small.

On the whole, however, both non-adiabatic crossing of the entrance channel pertaining to the $^4\Sigma$ potential occur at rather large distances and therefore we found in our test calculations that production of Si dications is not very efficient: the corresponding cross-sections are rather small and only involve shake-off processes without any CE crossing with the Rydberg states of the silicon cation.

The situation is, however, obviously modified when the CE process involves as entrance channel the $^2\Sigma$ potential of the atomic partners. The corresponding results are given by the curves of Fig. 3 where we have included only the crossing allowed by the approximate form of equation (B16) driven by the overlap integrals.

Over the range of collisional energies the silicon ions production is now given by much larger cross-sections since all crossings with the relevant PECs now occur also at smaller distances, as seen from the data in Fig. 1. The corresponding shake-off electron production starts at collision energies of about 1 eV since only the inner crossing between $^2\Sigma$ and $^1\Sigma$ curves is efficient, see equation (B16), enough to yield sizable cross-sections. The overall cross-sections remain, however, rather small since now the corresponding $H_{AB}(R)$ contribution is not very large in that region of distances.

The calculation of the corresponding partial rates, following equation (7) for all the CE processes discussed here, yields the values reported by Fig. 4.

As expected, the dominant contribution to the rates comes from the non-adiabatic crossing occurring in the inner region since the outer crossing yields shake-off processes with rather negligible cross-sections (see Fig. 4). The non-adiabatic processes guided by the interaction potential of the $^2\Sigma$ symmetry show to have fairly large non-adiabatic probabilities, especially for the production of initially excited, Rydberg states of the Si^+ cation, while the shake-off electron process yields much smaller rates as discussed earlier.

The total depletion probability of silicon atoms by collisional CE with He^+ cation, and over the range of temperature which is relevant for ISM conditions, is finally given by the data in Fig. 5.

The present data unequivocally show that the silicon atom losses by CE process with the helium cations in the astrophysical environment are dominated by the production of Si^+in electronically excited states corresponding to Rydberg excitation of its $|3l\rangle$ electrons, while the convergence to electron emission after the CE primary process is a less probable event with smaller rates by a factor of 20–30. On the other hand, our calculations of the relevant cross-sections also indicate that the rates have a clear temperature dependence and turn out to be smaller than the corresponding Langevin rates suggested in previous work (Le Teuff et al. 2000).

These findings are bound to have effects on our modelling of the ISM population evolution, for the atoms examined in this work, as we shall endeavour to show in the following section.

6 EFFECTS ON ISM EVOLUTIONARY CALCULATIONS

6.1 Constant temperature one-zone model

To discuss the effects of the new calculation on the ISM we have first developed a simpler model, similar to the one proposed in section 3.2 of Satta, Grassi & Gianturco (2013), that consists in a pseudo-time-dependent one-zone model which evolves from a given set of initial abundances at constant temperature and density. In spite of the simplicity of this model, the role of the calculations is mainly that of assessing the sensitivity effects produced by using our newly computed rates with respect to the earlier estimates existing in the literature (Le Teuff et al. 2000). As such, therefore, even the present simplified model is able to give us, as we shall show below, a realistic assessment of such effects. The reaction rates employed belong to the chemical network of Glover & Jappsen (2007), but in this case we replace their reaction labelled by R43 (Le Teuff et al. 2000) with our CE rate and, moreover, we add the shake-off reaction found in this work. The solver employed in our calculations is a standard DLSODES (Hindmarsh 1983) with a relative and absolute tolerance

Table 1. Coefficients of the fit of the reaction rates computed in this work, k_1 the single ionization channel and k_2 the double one. Units are $k_1 = k_2 = (\mathrm{cm^3 s^{-1}})$, $c_0 = (\mathrm{cm^3 s^{-1} K^{0.5}})$, $c_1 = (\mathrm{cm^3 s^{-1} K^{-1}})$, $c_2 = (\mathrm{cm^3 s^{-1} K^{-0.5}})$ and $c_0 = (\mathrm{cm^3 s^{-1}})$.

c_i	k_1	k_2
c_0	3.226 28(−13)	9.173 40(−15)
c_1	1.327 26(−16)	−1.220 25(−17)
c_2	4.1.533(−9)	5.916 40(−11)
c_3	−9.162 43(−13)	1.235 75(−13)

of 10^{-4} and 10^{-40}, respectively, which ensure a reliable numerical stability.

In our calculation, we have employed a fitting formula for the processes that have been included

$$k(T_\mathrm{g}) = c_0 {T_\mathrm{g}}^{0.5} + c_1 T_\mathrm{g} + c_2 {T_\mathrm{g}}^{-0.5} + c_3, \quad (8)$$

where c_i are the fit coefficients and T_g is the gas temperature. The coefficients for the single and the double ionization channels are listed in Table 1 for possible use by interested readers.

We first define $x_i = n_i/n_\mathrm{Htot}$ as the ratio between the number density of the ith species and the total abundance of hydrogen, that in our case is $n_\mathrm{Htot} = 10^3\,\mathrm{cm^{-3}}$. To determine the initial conditions of the test model we introduce an ionization background that at the beginning of the simulation ionizes the species in the ISM. From the photoionization cross-sections in Verner et al. (1996), we found that for an UV background with an impinging energy $E \gtrsim 20\,\mathrm{eV}$ (enough to ionize He), the cross-sections of Si, Si^+ and H photoionization are smaller than the He first photoionization cross-section. Conversely, oxygen and carbon cross-sections are larger than the He one. This suggests to a first approximation that only helium, carbon and oxygen are ionized, while Si is neutral. These non-standard initial conditions are chosen in order to increase the visibility of the effects that our calculations can have on the present, albeit simplified, ISM model.

The initial conditions of our model are then $x_{\mathrm{He^+}} = 9 \times 10^{-2}$, $x_{\mathrm{O^+}} = 2.56 \times 10^{-4}$, $x_{\mathrm{C^+}} = 1.2 \times 10^{-4}$ and $x_{\mathrm{H_2^+}} = 0.5$, while for silicon we chose two different values: *standard* with $x_\mathrm{Si} = 1.7 \times 10^{-6}$ and the *enriched* with $x_\mathrm{Si} = 1.7 \times 10^{-4}$ to investigate the effects of the new rates on two different ISM scenarios. To ensure the global charge neutrality of the cloud, we assume that the number density of the free electrons is evaluated by $n_{\mathrm{e^-}} = \sum_{i \in \mathrm{ions}} n_i$ only at the beginning of the simulation to guarantee the global charge neutrality of the chosen environment. We also add a cosmic rays ionization rate of $\zeta = 1.3 \times 10^{-17}\,\mathrm{s^{-1}}$, and we turn off the UV radiation during the calculation. All the species are computed without assuming the chemical equilibrium (i.e. each species has its own ODE to follow during the evolution).

We prepared a 20×20 grid of models changing two parameters: (i) a factor λ ranging from 10^{-2} to 10 which controls the amount of metals as $n_i = \lambda x_i n_\mathrm{Htot}$ for $i \in [\mathrm{O^+}, \mathrm{C^+}, \mathrm{Si}]$ and (ii) the temperature from 10 to 10^5 K that remains constant during the whole evolution. We let the system evolve for 10^4 yr and we plot in Fig. 6 for both *standard* and *enriched* scenarios the following quantity

$$\delta_\mathrm{Si} = \log\left[\frac{\left|n_\mathrm{Si}^\mathrm{new} - n_\mathrm{Si}^\mathrm{old}\right|}{n_\mathrm{Si}^\mathrm{old}}\right], \quad (9)$$

where $n_\mathrm{Si}^\mathrm{old}$ is the amount of Si at the end of the evolution ($t = 10^4$ yr) computed using the original Le Teuff et al. (2000) rate constant, while $n_\mathrm{Si}^\mathrm{new}$ is the same quantity but using our new rate coefficients. We stop the evolution at $t = 10^4$ yr because without any source of external ionization (except for the cosmic ray background) a larger integration time will result in a gas where each species is close to its neutral state (depending on the strength of the cosmic rays flux), and this will artificially cancel the effects of the present CE rates.

We note from both panels of Fig. 6 that in the temperature range $10 \lesssim T \lesssim 10^4\,\mathrm{K}$ the value δ_Si of equation (9) is higher, since

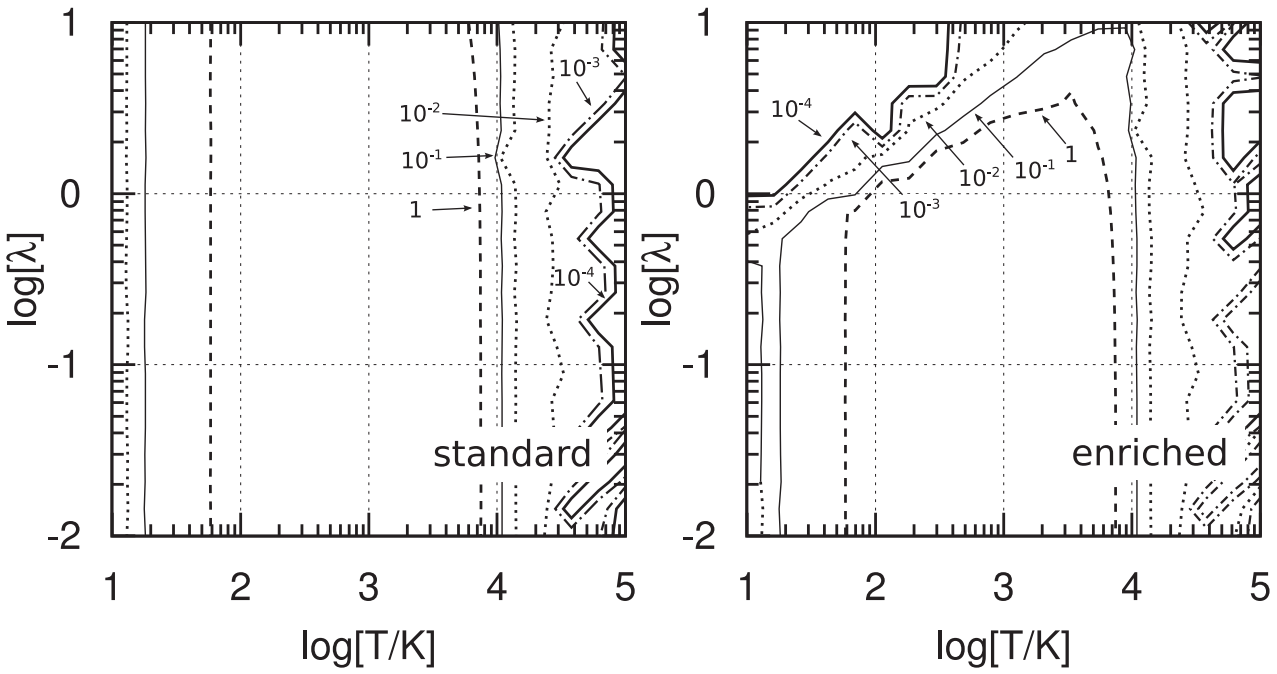

Figure 6. Contour plot as defined by equation (9) for standard Si^+ initial abundance (left) and enriched (right). The dashed line represents $\delta_\mathrm{Si} = 1$, solid thin 10^{-1}, dotted 10^{-2}, dash-dotted 10^{-3} and solid thick 10^{-4}. Each contour line is labelled by $\log(\delta_\mathrm{Si})$. See the text for details.

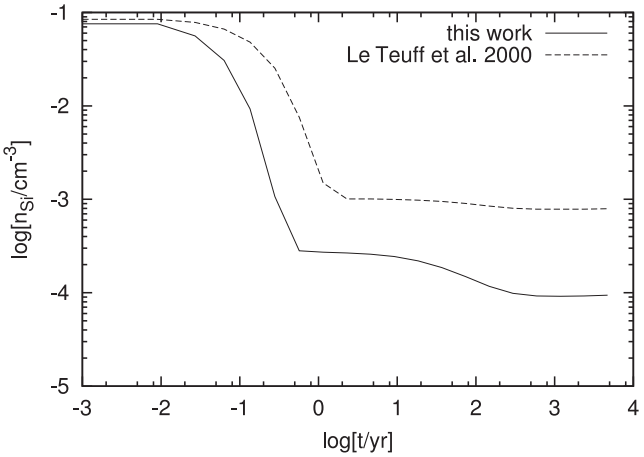

Figure 7. Evolution of Si number density for an *enriched* model with $T = 1.3 \times 10^3$ K and $\lambda = 0.127$. The dashed line represents the model run with the rate found in this work, while the solid line is the same evolution but using the rate of Le Teuff et al. (2000).

the differences between the Le Teuff et al. (2000) rate constants and ours are from the data in Fig. 5 markedly smaller. We also note that $\delta_{\rm Si}$ tends rapidly to zero for $T \gtrsim 10^4$ K, because in this region the difference between the old and the new rate is effectively cancelled by other efficient reactions involving Si that dominate such a temperature range. The small value of $\delta_{\rm Si}$ for $\log[\lambda] \gtrsim 0$ in the right-hand panel of Fig. 6 is derived from the Si/$H_{\rm tot}$ ratio which is controlled by λ, while He/$H_{\rm tot}$ is constant for any value of λ. In this region, the amount of Si is very high and it is not much affected by the rate of the process studied in this paper.

We also present in Fig. 7 the temporal evolution of a single *enriched* model with $T = 1.3 \times 10^3$ K and $\lambda = 0.127$ to show the changes of the Si number density with time: as expected, the model employing our rate destroys a smaller amount of Si compared with the model using the rate proposed by Le Teuff et al. (2000), since the present calculations found a reaction coefficient that is less efficient in forming Si^+, as shown in Fig. 5.

Finally, note that the reaction channel that produces the Si^{++} ion has a negligible effect on the amount of Si and Si^+ being produced in the present evolutionary model, and determines only a minor increase of the final number density of the doubly ionized silicon.

6.2 A more detailed model

We have further assessed the effects from the above comparison between our rate and the UMIST one in a more detailed one-zone model that includes also a photoionizing UV flux together with cooling and heating functions. These calculations are performed using KROME, a specialized code for astrochemistry (Grassi et al., in preparation), which partially follows the scheme adopted in Grassi et al. (2011). In particular, we track the chemical and thermal evolutions for a gas at constant density including the following physical processes: (i) collisional cooling from H_2 by using the model of Glover & Abel (2008), atomic cooling (H, He and ions) following Cen (1992) and fine-structure metal cooling (C, Si and ions) employing Maio et al. (2007) and Grassi et al. (2011). (ii) The heating is due to a soft photoionizing background that follows the distribution of Efstathiou (1992), Vedel, Hellsten & Sommer-Larsen (1994) and Navarro & Steinmetz (1997) for $z = 0$ and employing the rates of Verner et al. (1996) and Glover & Jappsen (2007). (iii) The same rates are employed also for the photoionization process.

As initial conditions we consider a hot ($T = 10^4$ K) ionized gas, with $n_{\rm H^+} = n_{\rm Htot} = 10^3\,{\rm cm^{-3}}$ and, by using the notation of Section 6.1, the other species are $x_{\rm He} = 0.1$, $x_{\rm C^+} = 1.2 \times 10^{-4}$, $x_{\rm O^+} = 2.56 \times 10^{-4}$ and $x_{\rm Si^+} = 1.7 \times 10^{-6}$. The total amount of free electrons at the beginning of the simulation is $n_{\rm e^-} = \sum_{i \in {\rm ions}} n_i$, i.e. the given environment is globally neutral. We solve the complete ODE system that represents the chemical networks of the reactions found (Glover & Jappsen 2007) and we track independently the evolution with time of each species.

The evolution of the abundance of Si with respect to the total amount of hydrogen is shown in Fig. 8 (left-hand panel), where the solid red line represents the model employing our new rates, while the dashed green line is the same model but with the original Langevin rate found in the UMIST data base (Le Teuff et al. 2000). From this plot, we note that our rates, as expected, appear to be less efficient in destroying the Si, a behaviour similar to the one found in the previous model (see Fig. 7). However, this difference becomes negligible at later evolutionary stages ($>2 \times 10^5$ yr) where the

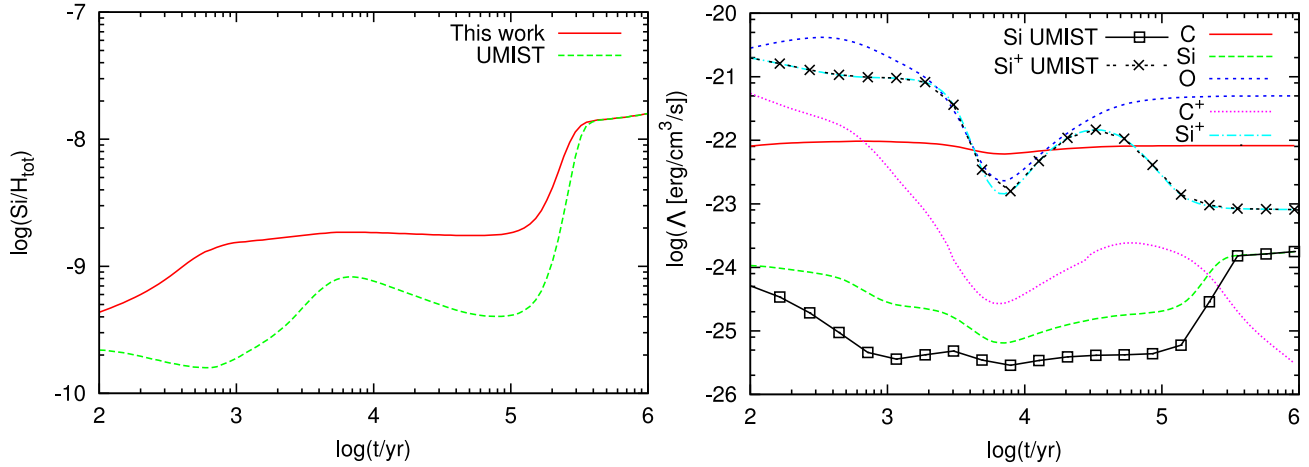

Figure 8. Left-hand panel: the evolution of the fractional abundance of Si as a function of the time for the model with the rates computed in this work (solid red) and the same model with the UMIST rate (dashed green). Right-hand panel: the contributions (Λ) to the metal cooling by each metal during the evolution of the model. The metals included are: carbon and its ion (solid red and small dotted magenta), oxygen (blue dashed), Si and Si^+ when employing our rate (green dashed and cyan dot–dashed) compared to the same model with the UMIST rate (solid with square and dashed with crosses).

recombination of the Si^+ with the electrons dominates the chemical network and the reaction rates studied in this work thus become less efficient within the model employed.

In addition, we would expect that a variation of the Si abundance will change the cooling efficiency. However, in our case the cooling by silicon plays a marginal role: this behaviour becomes clear when we compare the dashed line labelled Si with the solid lines with squares labelled Si UMIST in Fig. 8 (right-hand panel), which represents the contribution of the different terms of metal cooling Λ (see Maio et al. 2007; Grassi et al. 2011). The cooling from silicon seems to be now less important than oxygen (blue dotted) and carbon cooling (red solid and magenta small dotted), and for this reason its influence on the thermal evolution of the gas of the CE processes is shown to become negligible.

7 PRESENT CONCLUSIONS

The work described in this paper has been directed to study, via realistic quantum models of the nanoscopic dynamics, the losses of silicon atoms in dark clouds and in the inner regions of the PDR environments through charge transfer processes guided by the very likely presence of singly charged helium atoms.

The same general type of CE process has been studied before but chiefly via a simple Langevin-type of model, whereby no temperature dependence of the final rates was present (Le Teuff et al. 2000). One of the first conclusions of this work, however, is that the final computed models (see data in Fig. 5) exhibit a very marked dependence on the temperature, and therefore show a very different effect on any of the evolutionary studies within which our new rates are employed: the temperature dependence is therefore a significant new result suggested by the present calculations.

Additionally, our data described in the previous sections point out another physical effect which has not been discussed before and that is found here to have a significant bearing on the final cross-sections for CE processes: the large energy gain obtained by transferring the primary electron to the He cation causes the partner atom to be ionized into a manifold of electronically exited states, i.e. into a range of Rydberg excited Si^{+*} cations. From this new exit channel, it follows that the final Si^+ cations in the ground state will be obtained by further photon emission in the ISM environments, a possibility which was not considered before. Furthermore, the energy excess indicated above is also opening up another exit channel which we have discussed here in some detail, i.e. the production of silicon dications with the emission of one of its outer electron into the continuum.

The analysis of such channel at the molecular level, as discussed in the previous sections, shows however that the corresponding cross-sections are not very large and therefore its contribution to the silicon losses is not as important as that coming from the formation and radiative stabilization of Si^+ excited states.

The use of realistic interaction potential between partners, combined with a simple quantum discussion of both processes outlined above, allows us to obtain in the end rather clear changes from previous studies on the same process and to indicate the manifold of electronically excited silicon cations as the new significant result of the present calculation, together with the marked dependency of the actual local temperature of our final rates for Si^+ formation.

ACKNOWLEDGEMENTS

The computational support from the CASPUR Consortium through specific grants to the present project is gratefully acknowledged. One of us (TG) also thanks CINECA consortium for the awarding of financial support while the present research was carried out. SAY and AKB acknowledge financial support from the Russian Foundation for Basic Research (grant 13-03-00163).

REFERENCES

Becke A. D., 1993, J. Chem. Phys., 98, 5648
Belyaev A. K., 1993, Phys. Rev. A, 48, 4299
Boys S. F., Bernardi F., 1970, Mol. Phys., 19, 553
Cen R., 1992, ApJS, 78, 341
Clementi E., Raimondi D. L., 1963, J. Chem. Phys., 38, 2686
Demkov Y. N., Komarov I. V., 1966, Sov. J. Exp. Theor. Phys., 23, 189
Domcke W., 1991, Phys. Rep., 208, 97
Dunning T. H., 1989, J. Chem. Phys., 90, 1007
Efstathiou G., 1992, MNRAS, 256, 43P
Glover S. C. O., Abel T., 2008, MNRAS, 388, 1627
Glover S. C. O., Jappsen A.-K., 2007, ApJ, 666, 1
Glover S. C. O., Federrath C., Mac Low M.-M., Klessen R. S., 2010, MNRAS, 404, 2
Grassi T., Krstic P., Merlin E., Buonomo U., Piovan L., Chiosi C., 2011, A&A, 533, A123
Grassi T., Bovino S., Gianturco F. A., Baiocchi P., Merlin E., 2012, MNRAS, 425, 1332
Hindmarsh A. C., 1983, IMACS Tran. Sci. Comput., 1, 55
Jonhson R. E., 1982, Introduction to Atomic and Molecular Collisions. Plenum Press, New York
Kramida A., Ralchenko Y., Reader J., NIST A. S. D. Team, 2013, Technical report, NIST Atomic Spectra Database version 5.0. National Institute of Standards and Technology, Gaithersburg, MD, available at: http://physics.nist.gov/asd
Landau L. D., 1932, Phys. Z. Sous, 2, 46
Le Teuff Y. H., Millar T. J., Markwick A. J., 2000, A&AS, 146, 157
Maio U., Dolag K., Ciardi B., Tornatore L., 2007, MNRAS, 379, 963
Martin W. C., Zalubas R., 1983, J. Phys. Chem. Ref, Data, 12, 323
Miller W. H., 1970, J. Chem. Phys., 52, 3563
Miller W. H., Morgner H., 1977, J. Chem. Phys., 67, 4923
Navarro J. F., Steinmetz M., 1997, ApJ, 478, 13
Olson R. E., Smith F. T., Bauer E., 1971, Appl. Opt., 10, 1848
Satta M., Grassi T., Gianturco F. A., 2013, MNRAS, 429, 269
Stueckelberg E. C. G., 1932, Helv. Phys. Acta, 5, 370
Vedel H., Hellsten U., Sommer-Larsen J., 1994, MNRAS, 271, 743
Verner D. A., Ferland G. J., Korista K. T., Yakovlev D. G., 1996, ApJ, 465, 487
Wu Q., Van Voorhis T., 2005, Phys. Rev. A, 72, 024502
Yamasawa D., Habe A., Kozasa T., Nozawa T., Hirashita H., Umeda H., Nomoto K., 2011, ApJ, 735, 44
Zener C., 1932, Proc. R. Soc. A, 137, 696

APPENDIX A: MODELLING THE COMPOSITE LZ NON-ADIABATIC CROSSING MECHANISMS

The features of the interactions of Figs 1 and 2 clearly suggest that we must use a composite version of the LZ theory that considers the multiple crossings occurring between the entrance channel and the outgoing (CE and excitation) processes that produce the types of Si cations discussed before. To that end, we define here three classes of PEC following the pictorial view reported by Fig. A1: (i) the thick solid line represents the potential curve of $Si+He^+$ that is the initial state of the system, (ii) the dashed line is the electron shake-off channel leading to the Si^{++} +He state (CE plus ionization), while (iii) the many solid lines are the $[Si^+]^*$ +He states where the silicon is excited and singly ionized (CE plus excitation).

Each curve is labelled by an integer index that ranges from $k = 0$ (entrance channel) to $k = N$ (lowest Rydberg state), while $k = 1$ is

the electron shake-off curve. We consider a process to be a path over these curves following LZ-like composite crossings. In the standard LZ model, when a pair of curves that represent two given states cross, there is a probability P that the system changes its state so that the corresponding interaction moves from one curve to the other.

These crossings are represented in the figure as the filled black circles when the crossing probability is symmetric, while the empty circles indicate the cases where only the direct crossing is allowed (i.e. from solid to dashed line but not vice versa). It means that the probability for a collisional path to change from curve $k = 1$ to any state $k \neq 1$ is vanishing. This assumption describes the physical condition indicated before, i.e. we consider the ejection of an electron into the continuum to be an irreversible process not allowing recombination (Demkov & Komarov 1966). The crossings are labelled by a number that indicates the index k of a specific line crossed by $k = 0$, and a letter that represents the outer (A) or the inner (B) crossings with that curve.

In order to include the presence of two different outgoing PEC for the ^{2}P silicon states ($J = 1/2$ and $3/2$), the calculations count the same crossing twice, but since we cannot evaluate the actual shift of the two close states, we model the crossing of these curves as the crossing of each curves' couple that are taken to be infinitely close (i.e. negligibly shifted). Under this virtual shift assumption, and since the LZ probability for a given crossing depends on the shape and the position of the two intersecting PECs, the probability of a transition at avoided crossing for the $J = 1/2$ curve is the same of the $J = 3/2$ one, and in the composite LZ model discussed in this section the split curves will be independently included. The only difference is that the outgoing probabilities of the $J = 1/2$ and $3/2$ states are summed to obtain a single probability for the given ^{2}P component. This treatment is equivalent to including the effects from the J multiplicity in an approximate manner, i.e. not directly in the C coefficients of equation (B5) but only after the transitions with Si Ps states in the entrance channels as discussed in Appendix B1.

The whole process can be seen as an evolution that starts from the curve $k = 0$ on the right-hand side, then reaches one of the path's inversion points PI_k on the left (diamonds), and then returns back in order to exit from the right-hand side on a given curve. In Fig. A1 we show as an example, a path (red line) that first remains on the curve $k = 0$ and misses the crossings at 1A and 2A, then changes to another curve (to $k = 3$) at 3A and returns to the $k = 0$ channel at 3B. After this point it crosses to $k = 2$ at 2B and reaches the path

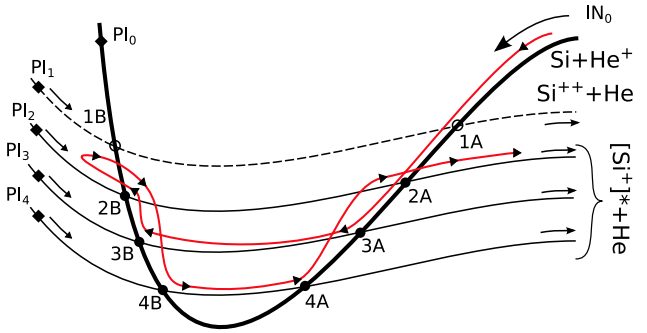

Figure A1. Pictorial view for the composite LZ approach. The thick solid line represents the potential curve of the system with ionized helium, the dashed line is the potential curve with the double-ionized silicon, and the remaining solid lines are the curves where the silicon is ionized and excited. The red line indicates a path of the process, while the black dots are the crossing points with symmetric (filled) and non-symmetric (empty) crossing probability. Finally, the path inversion points are indicated by the black diamonds. See the text for further details.

inversion point PI_2. On the way back the path returns to $k = 0$ at 2B, misses the crossing at 3B, but changes curve at 4B. Analogously, from $k = 4$ it returns to $k = 0$ at 4A, misses the crossing at 3A and exits from $k = 2$ at 2A. The composite probability of exiting from $k = 2$ following this trajectory is $P_{2\mathrm{in}} = \bar{P}_{1A}\bar{P}_{2A}P_{3A}P_{3B}P_{2B}$ on the way in, while $P_{2\mathrm{out}} = P_{2B}\bar{P}_{3B}P_{4B}P_{4A}P_{2B}\bar{P}_{3A}P_{2A}$ on the way out, where $\bar{P} = 1 - P$ and represents a missed crossing, i.e. for the partners to remain on a given PEC during their interaction. The composite probability of following this path is given by $P_{2\mathrm{in}} \times P_{2\mathrm{out}}$. It is clear that the total probability of exiting from $k = 2$ is given by the sum of all the composite probabilities of the paths that end in $k = 2$; although in this example we have shown only one of the probabilities.

For the sake of clarity, we divide the problem of calculating the probability $\hat{P}$ of reaching the exit on a given curve into two parts: (i) the composite probability of the paths that enter the curve $k = 0$ and reach PI_k, described below and (ii) the composite probability of the paths which, after any inversion point PI_k, exit from the ℓth curve, as discussed below.

A1 The composite LZ crossings on the way in

The probability of reaching the path inversion point PI_0 from the initial PEC of the entrance channel is given by

$$P_0 = \prod_{i=1}^{N} \bar{P}_{iA}\bar{P}_{iB} + \sum_{j=2}^{N}\left[\left(\prod_{i=1}^{j-1}\bar{P}_{iA}\right)P_{jA}P_{jB}\left(\prod_{i=1}^{j-1}\bar{P}_{iB}\right)\right], \quad \text{(A1)}$$

where the first part represents a path that misses all the crossings and remains always on $k = 0$, and the second part is the sum of the composite probabilities of the paths that miss the first $j - 1$ crossings, then follow the jth curve and then return to $k = 0$ and remain on that PEC.

Analogously, the probability of reaching PI_1 is given by

$$P_1 = \prod_{i=1}^{N}\bar{P}_{iA}\prod_{i=2}^{N}\bar{P}_{iB}P_{1B} + \sum_{j=2}^{N}\left[\left(\prod_{i=1}^{j-1}\bar{P}_{iA}\right)P_{jA}P_{jB}\left(\prod_{i=2}^{j-1}\bar{P}_{iB}\right)P_{1B}\right] + P_{1A}. \quad \text{(A2)}$$

Note that in this case (compare this expression with equation A1), we introduce the term P_{1A} that is simply the probability of the path to move from $k = 0$ to 1, since this process is not reversible and the only crossing occurs at 1A.

Finally, we define the composite probability for a path to reach $\mathrm{PI}_{k>1}$ as given by

$$P_k = \left(\prod_{i=1}^{N}\bar{P}_{iA}\right)\left(\prod_{i=k+1}^{N}\bar{P}_{iB}\right)P_{kB} + \sum_{j=k+1}^{N}\left[A_1^{j-1}P_{jA}P_{jB}B_{k+1}^{j-1}P_{kB}\right] + \left(\prod_{i=1}^{k-1}\bar{P}_{iA}\right)P_{kA}\bar{P}_{kB}, \quad \text{(A3)}$$

with $A_\alpha^\beta = \prod_{i=\alpha}^{\beta}\bar{P}_{iA}$ and $B_\alpha^\beta = \prod_{i=\alpha}^{\beta}\bar{P}_{iB}$ for a more compact notation. The above equation (A3) is analogous to equation (A2), but here the last term represents a path that misses all the crossings before reaching kA, and afterwards remains on the kth PEC.

Now we have all the composite probabilities P_k of reaching PI_k from the initial $k = 0$ curve, and they must satisfy $\sum_{k=0}^{N} P_k = 1$ since the total probability is a constant: this is always verified in the present calculations.

A2 The composite LZ crossings on the way out

The way out is a more complex situation because we must now sum the contributions from all the curves and not only from $k = 0$ as we have previously done. More in general, the composite probability for a path exiting from the ℓth curve is

$$\hat{P}_\ell = P_0 C_{0\ell} + \sum_{k=2}^{N} P_k C_{k\ell}, \tag{A4}$$

where $C_{0\ell}$ is the contribution of the PEC $k = 0$ to the crossing into the ℓth PEC. It must be multiplied by the probability P_0 calculated at the path inversion point PI_0. Analogously, the contribution for the paths coming from $\mathrm{PI}_{k>1}$ to reach the path ℓ is given by the various $C_{k\ell}$ weighted by the kth probability at PI_k. The contribution of $k = 1$ to the ℓth curve is $C_{1\ell} = 0$, since the electron recombination process is initially excluded, and then a path on the curve $k = 1$ remains on it until the exit. Note that $\hat{P}_k$ represents the probability at the path inversion point PI_k, while $\hat{P}_k$ is the probability at the kth exit point, and, by definition, it must also satisfy that $\sum_{k=0}^{N} \hat{P}_k = 1$.

A2.1 Contributions to the curve $\ell = 0$

In equation (A4) we have indicated that the contribution of the PEC $k = 0$ crossing into the $\ell = 0$ exit point is

$$C_{00} = \left(\prod_{i=1}^{N} \bar{P}_{iA} \bar{P}_{iB} \right) + \sum_{j=2}^{N} \left[B_1^{j-1} P_{jB} P_{jA} A_1^{j-1} \right]. \tag{A5}$$

The first part of equation (A5) is a path that remains on the PEC labelled by zero from the path inversion point PI_0 to the exit, and the second term indicates a path from the curve $k = 0$ that crosses at jB to return on the same curve at jA, and then misses all the crossings until the exit.

For $k > 1$ the contributions to the exit curve $\ell = 0$ are

$$C_{k0} = P_{kB} \left(\prod_{i=k+1}^{N} \bar{P}_{iB} \right) \left(\prod_{i=1}^{N} \bar{P}_{iA} \right) + P_{kB} \sum_{j=k+1}^{N} \left[B_{k+1}^{j-1} P_{jB} P_{jA} A_1^{j-1} \right] + \bar{P}_{kB} P_{kA} \left(\prod_{i=1}^{k-1} \bar{P}_{iA} \right), \tag{A6}$$

where the first and the second terms are analogous to the first and the second terms of equation (A5) except for the fact that now the origin of the path is $k > 1$, hence it is necessary to introduce the P_{kB} terms which indicate the probability of crossing from the kth curve to the curve labelled as zero. Conversely, when the first crossing is missed the path follows the PEC labelled zero at the point kA, and it remains there until the exit.

A2.2 Contributions to the curve $\ell = 1$

We also need to define the contributions to the crossing into the PEC labelled as $\ell = 1$. From PI_0 we have

$$C_{01} = \left(\prod_{i=1}^{N} \bar{P}_{iB} \right) \left(\prod_{i=2}^{N} \bar{P}_{iA} \right) P_{1A} + \sum_{j=2}^{N} \left[B_1^{j-1} P_{jB} P_{jA} A_2^{j-1} \right] P_{1A} + P_{1B}, \tag{A7}$$

where the first and the second terms are similar to equation (A5) except that the path changes the PEC labelled as zero at 1A. The last term is the path that after the crossing 1B follows the curve $\ell = 1$ till its exit. For the same reason, we also have

$$C_{11} = 1. \tag{A8}$$

Finally, a generic PEC $k > 1$ contributes to crossing into the PEC with $\ell = 1$ as

$$C_{k1} = P_{kB} \left(\prod_{i=k+1}^{N} \bar{P}_{iB} \right) \left(\prod_{i=2}^{N} \bar{P}_{iA} \right) P_{1A} + P_{kB} \sum_{j=k+1}^{N} \left[A_{k+1}^{j-1} P_{jB} P_{jA} B_2^{j-1} P_{1A} \right] + \bar{P}_{kB} P_{kA} \left(\prod_{i=2}^{k-1} \bar{P}_{iA} \right) P_{1A}, \tag{A9}$$

which is similar to C_{k0} but each term needs to be multiplied by the probability P_{1A} of abandoning the potential labelled as zero of exiting following the potential labelled as $\ell = 1$.

A2.3 Contributions to the curve $\ell > 1$

In the more general expression for the various contributions $C_{k\ell}$ to the exit point $\ell > 1$, we have that for $k = 0$

$$C_{0\ell} = \left(\prod_{i=1}^{N} \bar{P}_{iB} \right) \left(\prod_{i=\ell+1}^{N} \bar{P}_{iA} \right) P_{\ell A} + \sum_{j=\ell+1}^{N} \left[B_1^{j-1} P_{jB} P_{jA} A_{\ell+1}^{j-1} \right] P_{\ell A} + \left(\prod_{i=1}^{\ell-1} \bar{P}_{iB} \right) P_{\ell B} \bar{P}_{\ell A}, \tag{A10}$$

it is the general case of equation (A9) described above, except for the third term representing a path that avoids all the crossings until the ℓB one and then follows on the ℓth potential.

When $k = 1$ the contribution is

$$C_{1\ell} = 0, \tag{A11}$$

since a path which follows the energy curve $k = 1$ can contribute only to the $\ell = 1$ crossing because the probability of re-capturing the electron is taken to be as a vanishing one.

Finally, if $k > 1$ the contribution is given by

$$C_{k\ell} = P_{kB} \left(\prod_{i=k+1}^{N} \bar{P}_{iB} \right) \left(\prod_{i=\ell+1}^{N} \bar{P}_{iA} \right) P_{\ell A} + P_{kB} \sum_{j=M}^{N} \left[B_{k+1}^{j-1} P_{jB} P_{jA} A_{\ell+1}^{j-1} \right] P_{\ell A} + \left| \bar{P}_{kB} P_{kA} \left(\prod_{i=\ell+1}^{k-1} \bar{P}_{iA} \right) P_{\ell A} \right|_{k>\ell} + \left| \bar{P}_{kB} \bar{P}_{\ell A} \right|_{k=\ell} + \left| P_{kB} \left(\prod_{i=k+1}^{\ell-1} \bar{P}_{iA} \right) P_{\ell B} \bar{P}_{\ell A} \right|_{k<\ell}, \tag{A12}$$

where $M = \max(k + 1, \ell + 1)$. The first two terms have meaning similar to the corresponding terms in equation (A9), while the last

part of equation (A12) depends on the values of k and ℓ as indicated by the subscripts.

All the previous equations from (A5) to (A12) allow us to compute the different final composite probabilities $\hat{P}_k$ for each PEC shown in equation (A4), although we shall describe their detailed use in the following appendix.

APPENDIX B: CALCULATING CE TRANSITION PROBABILITIES

B1 Rydberg states

As shown in the next appendix, the probability for the occurrence of each CE process for the case of the bound final states can be approximately expressed in terms of non-adiabatic transition probabilities after passing every crossing between the various diabatic PECs, as illustrated in Fig. 1. Every p_{jk} represents a probability to make a transition from one adiabatic state to another adiabatic state after a single traverse of a non-adiabatic region associated with the crossing diabatic states j and k. Obviously, a non-adiabatic transition probability p_{jk} has a simple relation with a probability P_{jk} to make a transition from a diabatic state j to a diabatic state k after a single traverse of the same non-adiabatic region, that is,

$$P_{jk} = 1 - p_{jk}. \tag{B1}$$

The probabilities for each CE process are treated as a multitude of single and independent crossings between the initial diabatic PEC $j = 0$ and a final diabatic PEC $k = f$. Transition probabilities p_{jk} can then be calculated within the Landau–Zener–Stueckelberg approximation (Landau 1932; Stueckelberg 1932; Zener 1932) given by

$$p_{jk}(E, b) = \exp\left(-\frac{\xi_{jk}}{v_b(R_x)}\right), \tag{B2}$$

where

$$\xi_{jk} = \frac{2\pi H_{jk}^2}{\hbar \left| H_{jj}^{'} - H_{kk}^{'} \right|_{R_x}} \tag{B3}$$

is the LZ parameter for the relevant non-adiabatic region. Here, H_{jj} and H_{kk} are the diagonal elements of the Hamiltonian matrix in a diabatic representation, which in fact correspond to different diabatic PECs $V_0(R)$ and $V_f(R)$, see Fig. 1. The term R_{x_i} is the interatomic distance at which the ith crossing occurs, while $v_b(R_{x_i})$ is the relative radial velocity between the two atoms at the ith crossing point for a given choice of the impact parameter b and the collision energy E:

$$v_b(R_{x_i}) = v_0 \sqrt{1 - \frac{V(R_{x_i})}{E} - \frac{b^2}{R_{x_i}^2}}. \tag{B4}$$

The term v_0 is now the asymptotic velocity and $V(R)$ the relevant PEC for the partners. The argument of the square root defines the maximum value of the impact parameter b for each R and $V(R)$, beyond which the relative transition probability is zero.

The key point in applications of the LZ model is calculation of the off-diagonal matrix element $H_{jk} = \langle \Psi_j | H | \Psi_k \rangle$, H being the electronic fixed-nuclei Hamiltonian, $|\Psi_j\rangle$ and $|\Psi_k\rangle$ being many electron total wavefunctions. CE with ion excitation equation (3), as well as CE with ionization (2), are essentially two-electron-transition-based processes in contrast to a single-electron-transition CE process (1). This means that at least two electrons change their states during a collision: one transfers from the ground state of Si to the ground state of He^+, while another electron goes from the ground state of Si into an excited state of Si^+. The CE with ion excitation process has been studied by Belyaev (1993) for a similar collision process, $Hg + He^+ \rightarrow Hg^{+*} + He$. It has been found that the off-diagonal many electron matrix elements H_{jk} can be written in terms of single-electron matrix elements

$$H_{jk} = C \left[S_{jk}^{(2)} h_{jk}^{(1)} + S_{jk}^{(1)} h_{jk}^{(2)} \right], \tag{B5}$$

where C is a coefficient which accounts for possible contributions from fine-structure terms if included into the couplings (see Belyaev 1993), otherwise C can be put to unity. In case of the CE with ion excitation process (equation 3) the single-electron matrix elements read

$$h_{jk}^{(1)} = \langle \phi_{\rm Si}(1) | V_{{\rm e}_1\,{\rm He}^+} | \phi_{\rm He}(1) \rangle, \tag{B6}$$

$$h_{jk}^{(2)} = \langle \phi_{\rm Si}(2) | V_{{\rm e}_2\,{\rm He}^+} | \phi_{{\rm Si}^{+*}}(2) \rangle, \tag{B7}$$

where $V_{{\rm e}\,{\rm He}^+}$ is an interaction potential of an electron with a helium cation and

$$S_{jk}^{(1)} = \langle \phi_{\rm Si}(1) | \phi_{\rm He}(1) \rangle, \tag{B8}$$

$$S_{jk}^{(2)} = \langle \phi_{\rm Si}(2) | \phi_{{\rm Si}^{+*}}(2) \rangle \tag{B9}$$

are the single-electron overlap integrals, $|\phi\rangle$ being single-electron coordinate wavefunctions. Note that the off-diagonal matrix elements H_{jk} of equation (B5) are expressed as a sum of two terms because of two active electrons changing their wavefunctions during a collision. It is also worth to point out that the operator which determines these terms is a single-electron operator, that is, a potential energy operator for an interaction of an electron with He^+, but not the electronic Hamiltonian any more. The above overlap integral $S_{jk}^{(2)}$ is always non-zero when the Si^{+*} ion is a (^{2}P) state and the entrance channel describes a Si(^{3}P) state, while the $S_{jk}^{(1)} \times h_{jk}^{(2)}$ integral is disregarded as proposed by Miller & Morgner (1977).

The single-electron exchange matrix elements $h_{jk}^{(1)}$ defined by equation (B6) are the elements which determine single-electron CE processes: for example, the process of equation (1). They have been intensively studied for a long time, and a semi-empirical formula for one electron exchange has been given by Olson, Smith & Bauer (1971; see also Jonhson 1982), which in our case yields

$$h_{jk}^{(1)}(R) = DR\,{\rm e}^{-\beta R}, \tag{B10}$$

with

$$D = \sqrt{I_{\rm Si}}\sqrt{I_{\rm He}}\left(\sqrt{I_{\rm Si}} + \sqrt{I_{\rm He}}\right)\Big/\sqrt{2},$$

$$\beta = 0.86\left(\sqrt{I_{\rm Si}} + \sqrt{I_{\rm He}}\right)\Big/\sqrt{2}. \tag{B11}$$

The effective ionization energies have been calculated as a function of the effective nuclear charge $Z_{\rm eff}$ as $I = 0.5 Z_{\rm eff}^2$. We have considered only the core electrons as shielding the nucleus and have been using the data of Clementi & Raimondi (1963) to obtain a final effective nuclear charge of silicon and helium, respectively. It is worth to point out that the single-electron exchange matrix element $h_{jk}^{(1)}$ is multiplied by the overlap integral $S_{jk}^{(2)}$, so this product is only non-zero when the overlap integral $\langle \phi_{\rm Si} | \phi_{{\rm Si}^{+*}} \rangle$ is non-zero, i.e. for crossings of the entrance channel, Si($3p^2$) + He^+, with the exit diabatic channels which asymptotically correspond to $Si^+(n{\rm p}) + {\rm He}$, that is, for the P states of a silicon cation. For better clarity, the data in Fig. 1 show by thick lines which crossings will be allowed, by

equation (B5), between the $^2\Sigma$ state of the entrance channel and the manifold of Rydberg states of the exit channel $(SiHe)^{+*}$ reported by the next figure. It clearly shows a reduced number of crossings to be used within the calculations outlined in the next appendix. All of them, however, still refer to one component of the ^2P state of the silicon partner and therefore additional contribution from the PECs originating from the two components mentioned before shall have to be considered when calculating the crossing probabilities. For a lack of better data, the crossing will be increased in number but will refer to simply shifted PEC, as mentioned before.

The product $S^{(1)}_{jk} \times h^{(2)}_{jk}$ of equation (B5) has been suggested by Miller & Morgner (1977) to be negligible, so we shall not include it in the present calculations, given the general simplicity of our modelling.

Thus, the required non-adiabatic transition probabilities p_{jk} and, hence, the probabilities P_{jk} equation (B1) for transitions between diabatic states, can be calculated within the LZ model by means of equation (B2) in each non-adiabatic regions formed by the initial diabatic state $j = 0$ and a final diabatic state $k = f$ at the crossing distance R_x. The LZ parameters ξ_{jk} are calculated by means of equation (B3). The off-diagonal matrix elements $H_{jk} = H_{0f}$ are computed by means of equations (B10) and (B11). The corresponding overlap integrals $S^{(2)}_{jk}$ of equation (B9) are directly computed using the atomic orbitals of Si and Si^{+*} (see equation 3.3 of Miller & Morgner 1977). All quantities are taken at the crossing distances R_x. The probabilities are a function of both the collision energy and the impact parameter b.

B2 Bound-continuum transitions (CE plus ionization)

What is involved here is the evaluation of the width function within the local complex potential approximation over the range of action of the potential on the outgoing channel given by the process in equation (2), whereby an extra electron is emitted into its continuum

$$\Gamma(R) = 2\pi\rho(\epsilon)\left|V_{*,\epsilon}\right|^2, \tag{B12}$$

where $\rho(\epsilon)$ is the density of continuum states per unit energy and $V_{*,\epsilon}$ is

$$V_{*,\epsilon} = \langle \chi_\epsilon \Phi_{N-1} \left| V \right| \Psi_N \rangle, \tag{B13}$$

here Φ_{N-1} and Ψ_N are the electronic wavefunctions of the bound electrons in the out and in channels and χ_ϵ is the one electron orbital for the ejected electron. Note, that the operator V in equation (B13) is the electronic non-relativistic Hamiltonian, the same as treated before for the CE with ion excitation, $V = H$. If now one defines $\psi_\epsilon = \sqrt{\rho(\epsilon)}\chi_\epsilon$ and

$$\bar{V}_{*,\epsilon} = \langle \psi_\epsilon \Phi_{N-1} \left| V \right| \Psi_N \rangle, \tag{B14}$$

then

$$\Gamma(R) = 2\pi\left|\bar{V}_{*,\epsilon}\right|^2, \tag{B15}$$

and ψ_ϵ could be obtained via the Wenzel, Kraemer, Brillouin approximation (Miller & Morgner 1977). Their analysis finally provides an heuristic formula for $\Gamma(R)$

$$\Gamma(R) = 2\pi\left|\langle\psi_\epsilon|\phi_x\rangle\right|^2 \left|H_{AB}(R)\right|^2, \tag{B16}$$

where the overlap integral occurs between the ejected electron into the continuum, ψ_ϵ, and the ϕ_x outer bound electron in the Si atom: in our case, a $|3p\rangle$ electron. It has been computed here using the procedure obtained in Miller & Morgner (1977). The coupling matrix element which guides the shake-off electron emission process was also given by Olson et al. (1971) using a scaling formula which contains two parameters linked to the properties of the two active orbitals (Miller & Morgner 1977)

$$H_{AB} = D\, R \exp\left(-\beta R\right), \tag{B17}$$

where the parameters D and β are defined by equation (B11). Following Miller & Morgner (1977), who found similarity between excitation transfer and Penning ionization, we have used similar formulae equations (B10), (B11) and (B17) for the CE with ion excitation and the CE with ionization processes. At this stage, therefore, we already have the ingredients for evaluating the probability of the shake-off process at each impact parameter and collision energy E, where the asymptotic velocity $v_0 = \sqrt{2E/\mu}$ and μ is the relevant reduced mass

$$P(v, b) = 1 - \exp\left[-\int_A^B \frac{\Gamma(R)\mathrm{d}R}{\hbar v_b(R)}\right], \tag{B18}$$

where $A = R_{1A}$ and $B = \infty$ for outer crossings and $A = R_{TP}$ and $B = R_{1B}$ for inner crossings. The term $\Gamma(R)$ is given by equation (B16), as in Miller & Morgner (1977), R_{TP} is the position of the turning point, and R_{1A} and R_{1B} are the positions of the outer and inner crossings between the entrance channels and the $(SiHe)^{++}$ state.

The overlap integral in equation (B16) provides zero quasi-stationary width Γ in a stationary region of the entrance PEC, as it must be in the framework of the local complex potential approximation, which follows from the definition of Γ in the general theory of quasi-stationary states, see e.g. Domcke (1991).

It should be emphasized that the ground state of the double-ionized $SiHe^{++}$ cation is $^1\Sigma$, i.e. singlet, and hence, the electronic continuum states of $SiHe^{++}(^1\Sigma) + e^-$ are doublet. Since we treat the non-relativistic Hamiltonian, so the quasi-stationary widths are non-zero only for the doublet initial states, e.g. the $^2\Sigma$, as follows from equations (B14) and (B15). A spin–orbit operator would couple the entrance $^4\Sigma$, $^4\Pi$ channels with the doublet electronic continuum states of $SiHe^{++} + e^-$, but spin–orbit couplings are typically much smaller than non-relativistic couplings, if the latter are non-zero. Thus, the formulae (B16) and (B17) are applicable only for the doublet entrance channels. We can nevertheless compute such non-adiabatic transitions $^2\Sigma \leftarrow {}^4\Sigma$ using the same approximation discussed before in the relevant formulae, in order to test the present modelling of these processes. Since our present treatment does not explicitly include spin–orbit terms, our present numerical tests on their computed values found them to be negligible, as it was correctly expected from symmetry selection rules.

This paper has been typeset from a TEX/LATEX file prepared by the author.